Bacterial density as an unexpected factor regulating decomposition by soil oligotrophs

Alexandre Coche[a*], Tristan Babey[b], Alain Rapaport[c], Laure Vieublé Gonod[d], Patricia Garnier[d], Naoise Nunan[e,f], Jean-Raynald de Dreuzy[a]

[a] Univ Rennes, CNRS, Géosciences Rennes - UMR 6118, F-35000 Rennes, France

[b] Stanford University, Department of Earth System Science, Stanford, USA

[c] MISTEA, Univ. Montpellier, INRAE, Montpellier SupAgro, France

[d] UMR Ecosys, INRAE, AgroParisTech, Université Paris-Saclay, 78850, Thiverval Grignon, France

[e] Sorbonne Université, CNRS, IRD, INRAE, P7, UPEC, Institute of Ecology and Environmental Sciences—Paris, 4 place Jussieu, 75005 Paris, France

[f] Department of Soil & Environment, Swedish University of Agricultural Sciences, P.O. Box 7014, 75007 Uppsala, Sweden

[*] Corresponding author. *E-mail address*: alexandre.co@hotmail.fr (A. W. Coche)

Abstract

Bacterial decomposition of organic matter in soils is generally believed to be mainly controlled by the accessibility of bacteria to their substrate. The influence of bacterial metabolic traits on this control has however received little attention in highly heterogeneous spatial conditions under advective-dispersive transport of bacteria and substrates. Here, we develop a biochemical transport model to screen the interactive impacts of dispersion and metabolic traits on mineralization. We compare the model results with two sets of previously performed cm-scale soil-core experiments in which the mineralization of the pesticide

2,4-D was measured under well-controlled initial distributions and transport conditions. Bacterial dispersion away from the source of substrate induced a significant increase in 2,4-D mineralization, revealing the existence of a control of decomposition by the bacterial density, in addition to the accessibility to the substrate. This regulation of degradation by density becomes dominant for bacteria with an efficient uptake of substrate at low substrate concentrations (i.e. oligotrophs). The model output suggests that the distance between bacteria adapted to oligotrophic environments is a stronger regulator of degradation than the distance between substrate source and these bacteria. Such oligotrophs, commonly found in soils, compete with each other for substrate even under remarkably low population densities. The ratio-dependent Contois growth model, which includes a density regulation in the expression of the uptake efficiency, appears more versatile and accurate than the substrate-dependent Monod model. In view of their strong interactions, biochemical and transport processes cannot be handled independently but should be integrated, in particular when biochemical processes of interest are carried out by oligotrophs.

Keywords: biodegradation of organic matter; heterogeneous spatial distributions; biochemical reactive transport model; competition for substrate; metabolic traits; ratio-dependent growth

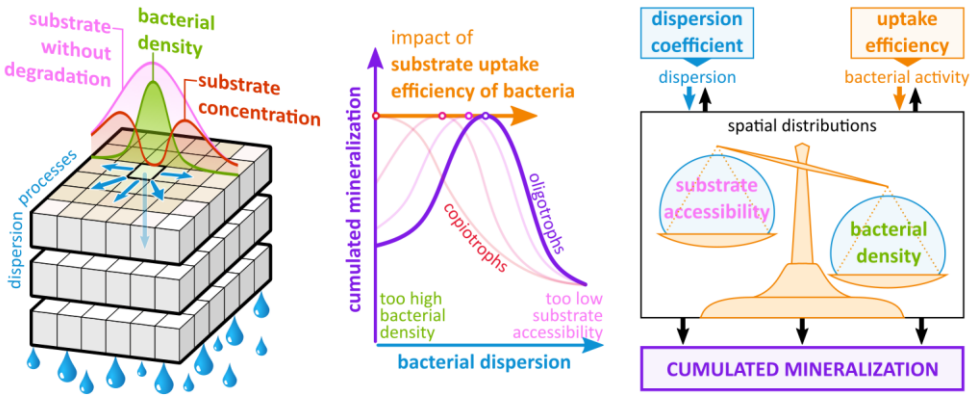

Highlights

- Biodegradation in soils results from strong biochemical and transport couplings
- Biodegradation depends on bacterial density, in addition to substrate accessibility

- Bacterial density regulation counterbalances substrate accessibility regulation
- Density regulation is enhanced for oligotrophic bacteria
- The ratio-dependent Contois model is relevant to represent this double regulation

1. Introduction

Organic carbon (C) is involved in most ecological functions provided by soils (Bünemann et al., 2018). Its cycling in soil is fundamentally driven by microorganisms. Soluble organic molecules can be taken up as substrates by specific populations of soil bacteria and degraded inside the cells by endoenzymes to provide carbon and energy, like it is the case for the 2,4-Dichlorophenoxyacetic acid (2,4-D) used in this study as a generic model compound (Don and Weightman, 1985; Pieper et al., 1988; Boivin et al., 2005). Bacterial degradation of soil C has generally been modeled with the Monod equation, where the specific substrate uptake rate is controlled by metabolic traits and substrate concentration (e.g. Monod, 1949; Sinton et al., 1986; Cheyns et al., 2010). Particularly, at the lowest substrate concentration, the specific uptake rate is linearly proportional to the substrate concentration. The proportionality factor is called here “maximum uptake efficiency” and reflects the maximal ability of the cell to effectively capture any substrate molecule that collides its membrane (Button, 1978, 1983). Each bacteria is assumed to be exposed to the whole substrate concentration of its environment, without any limitation by the population density (Lobry and Harmand, 2006).

The direct contact (exposure) between bacteria and substrate depends on their relative spatial distributions (Holden and Firestone, 1997; Nunan et al., 2007). Bacteria and substrate are both heterogeneously distributed as a result of numerous biotic and abiotic processes (Dechesne et al., 2014; Kuzyakov and Blagodatskaya, 2015). Their distributions interact with both transport processes, such as diffusion and percolation (Madsen and Alexander, 1982; Breitenbeck et al., 1988), and the bacterial activity itself, such as consumption and growth (Poll et al., 2006).

Clustered bacterial distributions, as observed at mm-scale for 2,4-D degraders (Vieublé Gonod et al., 2003), has been shown to decrease degradation rates when the distribution of substrate is homogeneous (Pallud et al., 2004; Dechesne et al., 2010). Yet, the role of bacterial metabolic traits on the impact of bacteria and substrate distributions on degradation remains mostly unknown especially when substrate and bacteria are heterogeneously and dynamically redistributed in soils over µm-to-cm scales by numerous spatial disturbances (Madsen and Alexander, 1982; Breitenbeck et al., 1988; König et al., 2020). We investigated the extent to which metabolic activity and transport processes can be handled independently or should be integrated to characterize, understand and predict degradation under various advective, diffusive and dispersive conditions. The simultaneous characterization of the impacts of biological metabolic traits and transport parameters through their mutual interactions is methodologically challenging. It requires several well-controlled experiments with specific distributions of substrate and degraders in comparable degradation conditions.

Among the scarce relevant datasets, we used the two sets of cm-scale soil-core experiments of Pinheiro et al. (2015, 2018) performed on similar repacked soil columns for the degradation of 2,4-D under different initial distributions and transport conditions. Mostly reported independently, they have shown first that the proximity between bacteria and heterogeneously distributed substrate sources, referred to as “accessibility” of bacteria to substrate (Dungait et al., 2012), is a strong control of mineralization. Substrate diffusion does not compensate for accessibility, as bacteria clusters located far from the substrate source are only exposed to highly diluted substrate (Babey et al., 2017). However, the hydrodynamic dispersion of both bacteria and substrate away from the substrate source strongly increased the bacterial degradation of the substrate that was not leached out (Pinheiro et al., 2018). We briefly introduce the experiments to show their potential to further explore bio-physical coupling within the unified quantitative framework proposed later in the article. The full experimental setting is presented in the supplementary materials (**Fig. S1** and **Table S1**) for the sake of completeness. Soil columns (**Fig. 1A**) were packed with two homogeneous or heterogeneous

arrangements of soil cubes, either sterilized, or hosting their indigenous soil microbial communities and amended with ^{14}C-labelled 2,4-D (**Fig. 1B,C**). Two sets of experiments, referred to as "hydrostatic" and "percolation" conditions, were performed respectively with only substrate diffusion (Pinheiro et al., 2015), or with additional substrate and bacterial advection and dispersion caused by water percolation (Pinheiro et al., 2018) (**Fig. 1C**). The mass of mineralized ^{14}C issued by the degradation of the labelled 2,4-D was monitored at the core scale during at least two weeks (**Fig. 1D**). There was a striking difference in the experimental results between the two conditions, in that the mineralization of the heterogeneous case (orange line) per unit of initial ^{14}C almost reached its homogeneous counterpart (purple line) in the percolation experiment (**Fig. 1D**, right), while it remained more than four times lower in the hydrostatic experiment (**Fig. 1D**, left). As the average distance between bacteria and the source of substrate increased with dispersion, resulting in reduced accessibility, the increase in mineralization is surprising. It suggests a control of mineralization by population density, which would enhance the activity of bacteria when they are diluted along with the substrate by the dispersive percolation events. The bacterial dilution and its positive effect on degradation seem to counterbalance the negative effect of the substrate dilution. While such regulations by bacterial density have not been yet considered in soils, presumably because of the extremely low apparent bacterial densities found in soils (Young et al., 2008), they are well known in bioreactors, where they are usually modeled by the ratio-dependent Contois growth law (Contois, 1959; Harmand and Godon, 2007).

To assess the relative importance of the mentioned processes and controls, we developed a quantitative approach to model the two sets of experiments within the same unified framework (section 2). We assessed the relevance of previously developed models, improved the calibration of a Monod-based model and investigated an alternative Contois-based model (section 3). We discussed the implication of the results on the controlling factors of soil organic carbon cycling, on the relevant bacterial growth models and on the possible bacterial strategies (section 4).

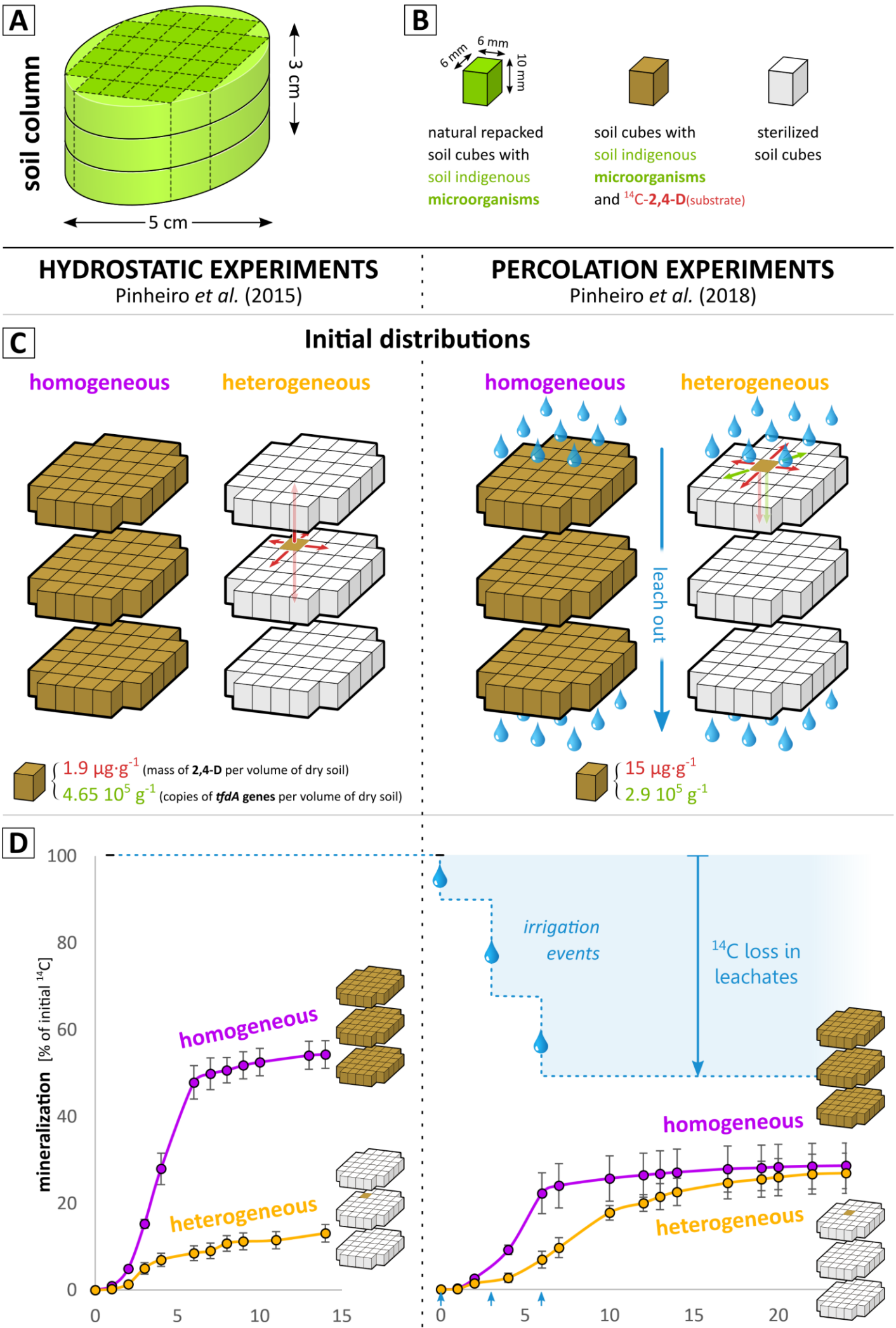
A
soil column
3 cm
5 cm
B
6 mm
6 mm
10 mm
natural repacked soil cubes with soil indigenous microorganisms
soil cubes with soil indigenous microorganisms and 14C-2,4-D(substrate)
sterilized soil cubes
HYDROSTATIC EXPERIMENTS
Pinheiro et al. (2015)
PERCOLATION EXPERIMENTS
Pinheiro et al. (2018)
C
Initial distributions
homogeneous
heterogeneous
homogeneous
heterogeneous
leach out
1.9 µg·g-1 (mass of 2,4-D per volume of dry soil)
4.65 10^5 g-1 (copies of tfdA genes per volume of dry soil)
15 µg·g-1
2.9 10^5 g-1
D
mineralization [% of initial 14C]
100
80
60
40
20
0
homogeneous
heterogeneous
0
5
10
15
irrigation events
14C loss in leachates
homogeneous
heterogeneous
0
5
10
15
20

Fig. 1. Experimental setup and mineralization (adapted from Pinheiro et al. (2018, 2015), permission for reproduction granted by Elsevier). (**A**) Sketch of soil columns experimental design and their decomposition into elementary soil cubes. (**B**) Description of the two categories of soil cubes. (**C**) Sketch of the hydrostatic and percolation experiments for the homogeneous and heterogeneous initial distribution of substrate and bacteria. The red and green arrows refer respectively to the 2,4-D and degrader reported displacements. (**D**) Experimental cumulated production of CO_2.

2. Models and methods

2.1. Biochemical model

The biochemical model extends the model published by Babey et al. (2017) (**Fig. 2**) to account for Contois growth law as an alternative of Monod's.

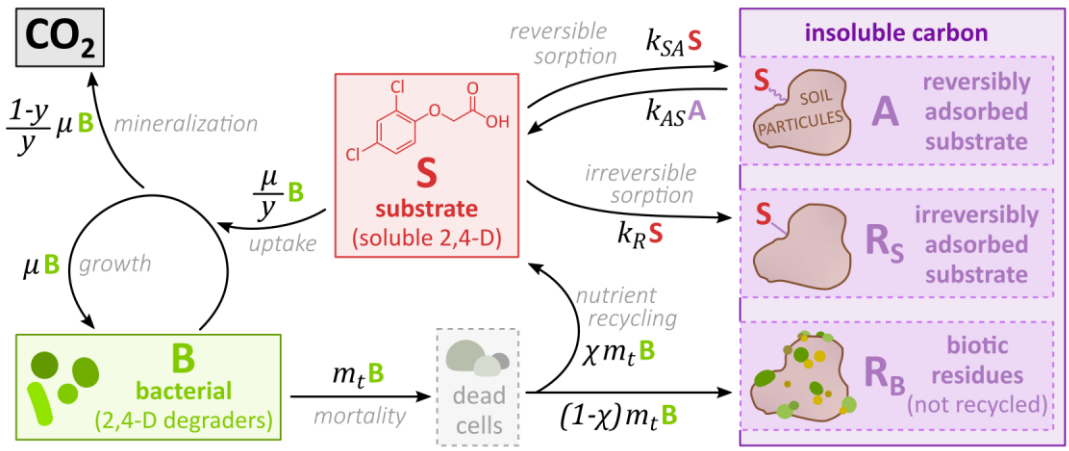

Fig. 2. Graphical representation of the biochemical model and carbon fluxes identified by the arrows. Under low substrate concentrations S, the specific uptake rate $(1/y)\cdot\mu$ becomes equal to $S\cdot(1/y)\cdot\mu_{max}/\kappa_M$, where $(1/y)\cdot\mu_{max}/\kappa_M$ is referred to as the "maximum uptake efficiency".

The $r(\cdot)$ notation expresses the reactional rates of the biochemical dynamics that are expressed as follows:

$$r(S) = k_{AS}\,A - k_{SA}\,S - k_R\,S - \frac{\mu}{y}B + m_t\,\chi\,B \tag{1}$$

$$r(A) = k_{SA}\,S - k_{AS}\,A \tag{2}$$

$$r(R_S) = k_R\,S \tag{3}$$

$$r(CO_2) = \frac{(1-y)}{y}\mu\,B \tag{4}$$

$$r(B) = \mu\,B - m_t\,B \tag{5}$$

$$r(R_B) = m_t(1-\chi)B \tag{6}$$

The dynamics of the specific growth rate μ are given, for the Monod-based model, by:

$$\frac{\partial\mu}{\partial t} = \alpha\left(\mu_{max}\frac{S}{\kappa_M + S} - \mu\right) \tag{7}$$

and, for the Contois-based model, by:

$$\frac{\partial\mu}{\partial t} = \alpha\left(\mu_{max}\frac{S/B}{\kappa_C + S/B} - \mu\right) = \alpha\left(\mu_{max}\frac{S}{\kappa_C B + S} - \mu\right) \tag{8}$$

where $\mu = 0$ at $t = 0$.

The soluble substrate S is either reversibly adsorbed to soil particles (pool A) or irreversibly adsorbed (pool R_S) (Eqs. (1), (2), (3)), or taken up by bacteria B (Eq. (1)) and metabolized into CO_2 (Eq. (4)) and new biomass B (Eq. (5)). k_{SA} and k_{AS} are the reversible sorption coefficients. k_R is the irreversible one. Bacteria death occurs at a constant rate m_t (Eq. (5)) and a fraction of the bacterial necromass is considered to return to the soluble substrate pool S to account for nutrient recycling (Eq. (1)), while the rest is transformed to biotic residues R_B (Eq. (6)). The adsorbed substrate and biotic residues form the pool of insoluble carbon $A + R_S + R_B$. The substrate S is consumed by bacteria B according to their specific uptake rate $(1/y)\cdot\mu$ expressed either by the substrate-dependent Monod growth law (Eq. (7)) (Monod, 1949) or by the ratio-dependent Contois growth law (Eq. (8)) (Contois, 1959). y is the yield coefficient and relates the specific uptake rate $(1/y)\cdot\mu$ to the specific growth rate μ. μ_{max} is the maximum specific growth rate. κ_M and κ_C are Monod and Contois constants respectively. The effective uptake is delayed by the accommodation rate α, which explicitly takes into account the "memory" effects of the bacteria when adapting to new conditions (Patarinska et al., 2000).

Over long time periods ($t \gg 1/\alpha$), μ follows the exact expression of the Monod or Contois equations. All modeled pools (S, B, CO_2, A, R_S and R_B) were expressed as carbon concentrations in µg·g^{-1} (mass of carbon per mass of dry soil) considering a soil water content of 0.205 g·g^{-1} (mass of water per mass of dry soil) corresponding to a water potential of -31.6 kPa (pF 2.5), an apparent density of the soil column of 1.3 10^3 g·l^{-1} (mass of dry soil per apparent soil volume) and an average bacterial dry weight of 2.8 10^{-13} g corresponding to 1.49 10^{-13} g of carbon per cell (Dechesne et al., 2010; Pinheiro et al., 2015). The moisture level (54%, volume of water per volume of pores) was such that oxygen was not considered a limiting factor for 2,4-D degradation.

2.2. Reactive transport model

The transport model extends the diffusion model of Babey et al. (2017) to the advective-dispersive processes explored in the experiments of Pinheiro et al. (2018). Bacterial leaching out and dispersion were observed only in the percolation experiments while the substrate was also reported to diffuse. Hydrodynamic leaching and dispersion were modeled independently, as resulting respectively from a bypass flow through large pores and a redistribution of saturation in the pore network. Bacteria and substrates were assumed to be transported with the same advective and dispersive parameters. This assumption did not significantly alter the results (**Fig. S3**). Coupled to the equations of the biochemical model ((1)-(8)), the full reactive transport model is given by:

$$\frac{\partial S}{\partial t} = r(S) + \nabla\left(d_{diff}\nabla S\right) + \; G\left(\nabla\left(d_{disp}\nabla S\right) - \nu\, S\right) \tag{9}$$

$$\frac{\partial B}{\partial t} = r(B) + G\left(\nabla\left(d_{disp}\nabla B\right) - \nu\, B\right) \tag{10}$$

$$\frac{\partial U}{\partial t} = r(U) \qquad \text{for } U = A,\ R_B,\ R_S \text{ and } CO_2 \tag{11}$$

where d_{diff} is the effective diffusion coefficient of S, d_{disp} is the effective dispersion coefficient of S and B and ν is their leaching rate. Note that the dispersion coefficient d_{disp} mostly affected the spreading of bacteria, given that substrate was mainly spread by diffusion, as noted in section 2.2 and confirmed by consistent results from equivalent models without hydrodynamic dispersion of S (**Fig. S4**). Effective diffusion and dispersion processes were assumed isotropic and uniform at the column-scale. Dispersion and leaching were active only during the observed 1-hour percolation events at days 0, 3 and 6 as controlled by the function G defined by:

$$\begin{aligned} G(t) &= 1 \quad t = [0\text{d} - 0\text{d}1\text{h}]; [3\text{d} - 3\text{d}1\text{h}]; [6\text{d} - 6\text{d}1\text{h}] \\ G(t) &= 0 \quad \text{otherwise.} \end{aligned} \tag{12}$$

No-flow boundary conditions were imposed on the edges of the soil core ($\nabla S = 0$ and $\nabla B = 0$) at any time outside of the percolation events. The transient evolutions of the water content and their effects on concentrations were not considered because of the short duration of the percolation events (1 h) and the absence of detectable effects on the experimental mineralization curve around the percolation events (**Fig. 1D**).

Concentration dynamics were simulated on a 3 × 6 × 6 regular mesh grid. Although the shape of the grid was slightly different from that of the cylindrical soil-core, it did not have any observable impact (Babey et al., 2017). We recall that substrate and bacteria were initially colocalized in the same cube(s). Each cube was considered to be physically, chemically and biologically homogeneous. Diffusion and dispersion were simulated using a finite-difference scheme (Iserles, 2009) and coupled with the biochemical model, itself solved by the 4th order Runge-Kutta integration method function of MATLAB (Shampine and Reichelt, 1997). The coupling between transport and biogeochemical models was achieved with a sequential non-iterative method. The time steps were smaller than the characteristic diffusion and reaction times to avoid any coupling issues.

2.3. Exploratory screening

Parameters and their values are listed in **Table 1**. Known parameters were set at their calibrated values by Babey et al. (2017). Explored parameters were screened within the theoretically and physically relevant ranges given by Babey et al. (2017) and calibrated through the screening. The four biological parameters primarily involved in the biological response of bacteria to the concentration of substrate, either $(1/y)\cdot\mu_{max}$, $(1/y)\cdot\mu_{max}/\kappa_M$, α and $B(t=0)$ for the Monod-based model or $(1/y)\cdot\mu_{max}$, $(1/y)\cdot\mu_{max}/(B(t=0)\cdot\kappa_C)$, α and $B(t=0)$ for the Contois-based model, were screened over 7 logarithmically-distributed values (**Table S2**). We recall that the "maximum uptake efficiency" $(1/y)\cdot\mu_{max}/\kappa_M$ characterizes the specific bacterial uptake of substrate at the lowest substrate concentration (Button, 1991), while the maximum specific uptake rate $(1/y)\cdot\mu_{max}$ characterizes the bacterial uptake at the highest substrate concentration. Note that the uptake yield y was fixed at its value calibrated by Babey et al. (2017), where it has been well identified. For the Contois-based model, the initial maximum uptake efficiency $(1/y)\cdot\mu_{max}/(B(t=0)\cdot\kappa_C)$ was screened in the same range as $(1/y)\cdot\mu_{max}/\kappa_M$. The accommodation rate α of the degrader response ranged from negligible delay of few minutes (α = 934 d^{-1}) to prolonged delay of around 10 days (α = 9.34 10^{-2} d^{-1}). $B(t=0)$ values were screened around the initial experimental measurements of *tfdA* gene copy number, assuming that one *tfdA* sequence corresponded to one bacterium. They ranged over two orders of magnitude to account for the uncertainty of the conversion of *tfdA* copy number into alive 2,4-D degraders (Bælum et al., 2006, 2008). In the uptake efficiency expression, bacterial density will also be expressed in $g\cdot l^{-1}$ (mass of bacteria per volume of water) for more direct comparison with the relevant literature.

The spatial distribution of bacteria observed at the end of the experiments could not be used to determine the effective dispersion coefficient d_{disp} (**Fig. S2**). While they qualitatively ascertained that bacteria were dispersed orthogonally to the percolation direction, experimental data were not sufficiently resolved to be used quantitatively. The dispersion coefficient was thus screened over 10 values ranging from no dispersion

(d_{disp} = 0) to complete instant homogenization of the soil core (d_{disp} = inf) (**Table S2**). The effective diffusion coefficient d_{diff} had been calibrated independently from percolation conditions (Pinheiro et al., 2015; Babey et al., 2017). The leaching rates ν were determined based on the experimental masses of leached ^{14}C (Pinheiro et al., 2018) (**Table 1**).

Detailed values for the screened parameters are listed in **Table S2**. The 62 426 simulations were performed sequentially in around 2 weeks on a server (2.2 GHz, 512 Go RAM).

Table 1.

Values and range of values of the reactive transport model. The effective dispersion coefficient d_{disp} applies only to heterogeneous percolation experiments. $B(t=0)$ is the initial density of bacteria in the natural cubes. It is considered 1.6 times smaller in the percolation experiments than in the hydrostatic experiments according to the initial experimental measurements.

Parameter description		Symbol	Unit	Fixed values and admissible ranges for screening
initial substrate concentration	hydrostatic experiments	$S(t=0)$	µg·g^{-1} (mass of substrate carbon per mass of dry soil)	0.825 [b]
	percolation experiments		µg·g^{-1}	6.52 [b]
reversible adsorption coefficient		k_{SA}	d^{-1}	0.09207
reversible desorption coefficient		k_{AS}	d^{-1}	4.361
irreversible adsorption coefficient		k_C	d^{-1}	0.01296
uptake yield		y	-	0.5206
maximum specific uptake rate		$(1/y)\cdot\mu_{max}$	d^{-1}	[0.0190 – 19.5]
uptake efficiency at the lowest substrate concentration		$(1/y)\cdot\mu_{max}/\kappa$ [a] *where* κ *is* κ_M *or* $B(t=0)\cdot\kappa_C$	g·µg^{-1}·d^{-1} (mass of dry soil per mass of bacterial carbon per unit of time)	[0.0152 – 159] [c]

accommodation rate		α	d^{-1}	[0.00934 – 934]
initial degrader population density	hydrostatic experiments	$B(t=0)$	$\mu g \cdot g^{-1}$ (mass of bacterial carbon per mass of dry soil)	[0.0161 – 1.61] [d]
	percolation experiments	$B(t=0)$	$\mu g \cdot g^{-1}$	[0.0101 – 1.01] [d]
mortality rate		m_t	d^{-1}	0.0602
nutrient recycling yield		χ	-	0.6010
effective diffusion coefficient		d_{diff}	$m^2 \cdot d^{-1}$	$1\ 10^{-5}$ [e]
effective dispersion coefficient		d_{disp}	$m^2 \cdot d^{-1}$	[0 – ∞]
leaching rates (days 0; 3; 6)	homogeneous experiments	ν	-	0.108; 0.226; 0.180
	heterogeneous experiments			0.107; 0.223; 0.178

[a] The half-saturation constant κ corresponds to κ_M for the Monod-based model and $B(t=0) \cdot \kappa_C$ for the Contois-based model (where $B(t=0)$ is the value from the hydrostatic experiments).

[b] The initial substrate concentration $S(t=0)$ is set equal to the ^{14}C-2,4-D concentration amended in the experiments.

[c] The values of $(1/y) \cdot \mu_{max}/\kappa$ correspond to ranges of [1.65 – 1.73 10^4] $l \cdot g^{-1} \cdot d^{-1}$ (volume of water per mass of bacteria per unit of time)

[d] The values of $B(t=0)$ correspond respectively to ranges of [1.48 10^{-4} – 1.48 10^{-2}] $g \cdot l^{-1}$ (mass of bacteria per volume of water) for the hydrostatic experiments and [9.24 10^{-5} – 9.24 10^{-3}] $g \cdot l^{-1}$ for the percolation experiments.

[e] The value of d_{diff} has been calibrated on a 3 × 6 × 6 grid in similar conditions (Babey et al., 2017).

2.4. Model to data comparison

The comparison between the results of the model and the experimental data was based on the core-scale data of mineralization deduced from the carbon mass m_{CO2} of $^{14}CO_2$ emissions:

$$m_{CO_2}(t) = \int_V CO_2(x,t)dx \tag{13}$$

with V the volume of the soil cores. Mineralization was expressed as the carbon mass of cumulated $^{14}CO_2$ emissions per initial carbon mass of ^{14}C-substrate S. Data-to-model adequacy was assessed for each of the experiments by a classical root-mean-square evaluation function J_q comparing the modeled mineralization of Eq. (4) to the measured mineralization at the n_q available sampling times t_i:

$$J_q = \left(\frac{1}{n_q} \sum_{i=1}^{n_q} \left(\frac{m_{CO_2,q}^{mod}(t_i) - m_{CO_2,q}^{data}(t_i)}{m_{S,q}(0)} \right)^2 \right)^{\frac{1}{2}} \tag{14}$$

where the index q identifies the experiment at hand. Indices 1, 2, 3 and 4 are respectively given to the homogeneous hydrostatic, heterogeneous hydrostatic, homogeneous percolation and heterogeneous percolation experiments. Discrepancies over the full set of experiments J_{1234} were thus expressed as:

$$J_{1234} = \left(\frac{1}{4} \sum_{k=1}^{4} J_k^2 \right)^{\frac{1}{2}} \tag{15}$$

Calibration was performed by minimizing J_{1234} in a classical least-square optimization using a parameter screening approach.

3. Results

3.1. Model calibration

All parameters of the reactive transport model (**Table 1**), except the effective dispersion coefficient d_{disp}, were previously calibrated on the sole hydrostatic experiments (Babey et al., 2017), corresponding to a minimal discrepancy between data and model (J_{12} = 0.023, **Fig. 3-A1** and **A2**). This pre-existing model was used to provide blind predictions of the percolation experiments, with the dispersion coefficient as an additional fitting parameter. It gave a reasonable prediction of mineralization in the homogeneous percolation experiment (J_3 = 0.038, **Fig. 3-A3**) but failed in the heterogeneous percolation experiment (J_4 = 0.151, **Fig. 3-A4**), no matter the dispersion. The smallest discrepancy J_4 was surprisingly obtained without any bacterial dispersion (d_{disp} = 0) in contradiction with the bacterial spreading observed in the experimental data (**Fig. S2**). The final predicted mineralization was at the highest when bacteria remained aggregated close to the substrate source. The highest predicted mineralization was however four times lower than the experimental data. The large gap to the data and the experimental bacterial spreading suggest that degradation might benefit more from a dispersion-related control than from the proximity of bacteria to the substrate source.

In order to investigate the capacity of the reactive transport model to fit both hydrostatic and percolation experimental data, the biological parameters ($(1/y)\cdot\mu_{max}/\kappa_M$, $(1/y)\cdot\mu_{max}$, α, $B(t=0)$) and the dispersion coefficient (d_{disp}) were calibrated on both hydrostatic and percolation experiments following the screening approach given in section 2.2 to minimize J_{1234}. The mineralization dynamics were adequately predicted in all four experiments with the biological parameter set giving the lowest overall discrepancy (J_{1234} = 0.032) and a non-zero dispersion coefficient (d_{disp} = 1.78 10^{-4} $m^2 \cdot d^{-1}$) (**Fig. 3**, **Table 2**). The non-zero dispersion coefficient indicates that the calibrated model accounts for a beneficial impact of bacterial dispersion on

degradation, seemingly necessary to successfully predict the high degree of degradation in the experimental data. Compared to the parameters calibrated on the sole hydrostatic experiments, the parameter set calibrated on both hydrostatic and percolation experiments also displayed a much higher maximum uptake efficiency $(1/y)\cdot\mu_{max}/\kappa_M$ = 26.5 $g\cdot\mu g^{-1}\cdot d^{-1}$ (mass of dry soil per mass of bacterial carbon per unit of time) (**Table 2**). The systematic exploration of the parameter space showed that higher maximum uptake efficiency was a common feature to the 1% best-fitting parameterizations to both hydrostatic and percolation experiments (smallest J_{1234}), with values of 159 and 26.5 $g\cdot\mu g^{-1}\cdot d^{-1}$, corresponding respectively to 1.73 10^4 and 2.89 10^3 $l\cdot g^{-1}\cdot d^{-1}$ (volume of water per mass of bacteria per unit of time). It underlines the essential role of the maximum uptake efficiency for modulating the impact of dispersion on degradation, further detailed and explained in section 3.2.3.

Table 2.

Parameters for the Monod-based model calibrated by the screening approach (section 2.2) on the hydrostatic experiments only (Babey et al., 2017) and on both hydrostatic and percolation experiments, and for the Contois-based model calibrated on both hydrostatic and percolation experiments.

Parameter symbol		Unit	Monod model calibration		Contois model calibration
			on the sole hydrostatic experiments	on both hydrostatic & percolation experiments	on both hydrostatic & percolation experiments
$(1/y)\cdot\mu_{max}$		d^{-1}	1.22	9.73	4.86
$(1/y)\cdot\mu_{max}/\kappa$ [a]		$g\cdot\mu g^{-1}\cdot d^{-1}$ (mass of dry soil per mass of bacterial carbon per unit of time)	2.65 [b]	26.5 [b]	2.65 [b]
α		d^{-1}	$9.341\ 10^{-1}$	$9.34\ 10^{-2}$	$9.34\ 10^{-2}$
$B(t=0)$	hydrostatic experiments	$\mu g\cdot g^{-1}$ (mass of bacterial carbon per mass of dry soil)	$1.61\ 10^{-1}$	$3.23\ 10^{-2}$	$3.76\ 10^{-1}$
	percolation experiments	$\mu g\cdot g^{-1}$	$1.01\ 10^{-1}$	$2.01\ 10^{-2}$	$2.34\ 10^{-1}$
d_{disp}		$m^2\cdot d^{-1}$	0 [c]	$1.78\ 10^{-4}$ [c]	10^{-5} [c]
J		-	0.079	0.032	0.022

[a] The half-saturation constant κ corresponds to κ_M for the Monod-based model and $B(t=0)\cdot\kappa_C$ for the Contois-based model (where $B(t=0)$ is the value from the hydrostatic experiments).

[b] Values of $(1/y)\cdot\mu_{max}/\kappa$ correspond respectively to $2.89\ 10^2$, $2.89\ 10^3$ and $2.89\ 10^2$ $l\cdot g^{-1}\cdot d^{-1}$ (volume of water per mass of bacteria per unit of time).

[c] The corresponding spreading values induced by the hydrodynamic dispersion (root-mean-square displacements) for each percolation events are respectively 0, 3.8 and 0.91 mm, to be compared to the 25 mm radius of the soil column.

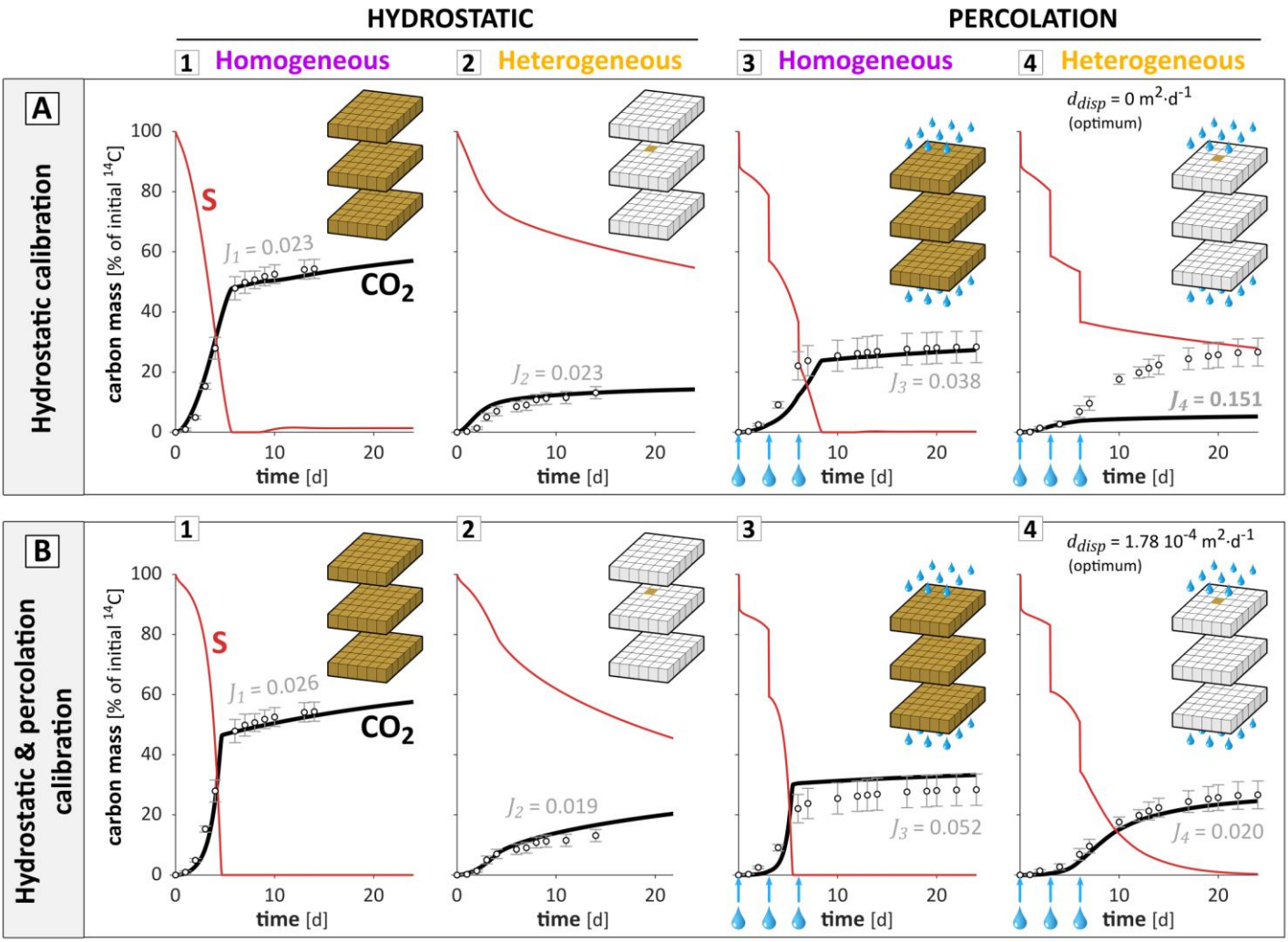

Fig. 3. Mineralization dynamics predicted with the Monod-based model calibrated on the hydrostatic experiment only (**A**) and on both hydrostatic and percolation experiments (**B**). The related experimental setups are indicated in the top right corner of each graph. The agreement between experiments and model is indicated by the value of discrepancy J displayed on top and can be visually assessed by the proximity between the black line and the dots representing respectively the model results and experimental data. The red line refers to the carbon mass of substrate remaining in the soil core. In the percolation experiments (**A3,4** and **B3,4**), around 51% of the initial mass of ^{14}C was lost through leaching at each percolation events (t = 0, 3 and 6 days, blue arrows). The carbon balance among the different pools is detailed in **Fig. S5**.

3.2. Exploration of the controls of degradation by substrate accessibility and bacterial density

The effect of dispersion on degradation widely differed between the two calibrated sets of biological parameters of the previous section 3.1. To explain this, we investigated more systematically the interactive impact of bacterial dispersion and bacterial traits on degradation, revealing its control by substrate accessibility and bacterial density.

3.2.1 Impact of dispersion on degradation

We used the mineralization at the end of the experimental time (day 24) as a proxy for degradation and determined its sensitivity to dispersion, depending on bacterial traits parameterization. **Fig. 4** shows the impact of the dispersion coefficient d_{disp} on the final predicted mineralization for the two calibrated biological parameter sets, all other parameters being kept constant (thick red and blue lines). The thin mauve lines correspond to parameterizations with the same maximum uptake efficiency $(1/y)\cdot\mu_{max}/\kappa_M$ but different maximum specific uptake rates $(1/y)\cdot\mu_{max}$, accommodation rates α and initial bacterial population densities $B(t=0)$. For the biological model calibrated on hydrostatic experiments and most parameterizations sharing the same maximum uptake efficiency, the final mineralization monotonously decreased with dispersion (**Fig. 4A**). For the model calibrated on both hydrostatic and percolation experiments and most parameterizations sharing the same maximum uptake efficiency, the final mineralization first increased, reached a maximum around $d_{disp} \approx 10^{-4}$ $m^2 \cdot d^{-1}$ and then decreased (**Fig. 4B**). The non-monotonous impact of dispersion on degradation remarkably highlights the existence of an optimal bacterial dispersion for which mineralization is the highest. The comparison between **Fig. 4A** and **Fig. 4B** suggests that the optimal dispersion value depends on the bacterial uptake efficiency. Note that, although the optimal dispersion value varied with time due to the dynamics of spatial distributions of bacteria and substrate (**Fig. S6**), it tended towards a limit that was mostly reached within 4 to 7 days and is thus represented at day 24 on **Fig. 4**.

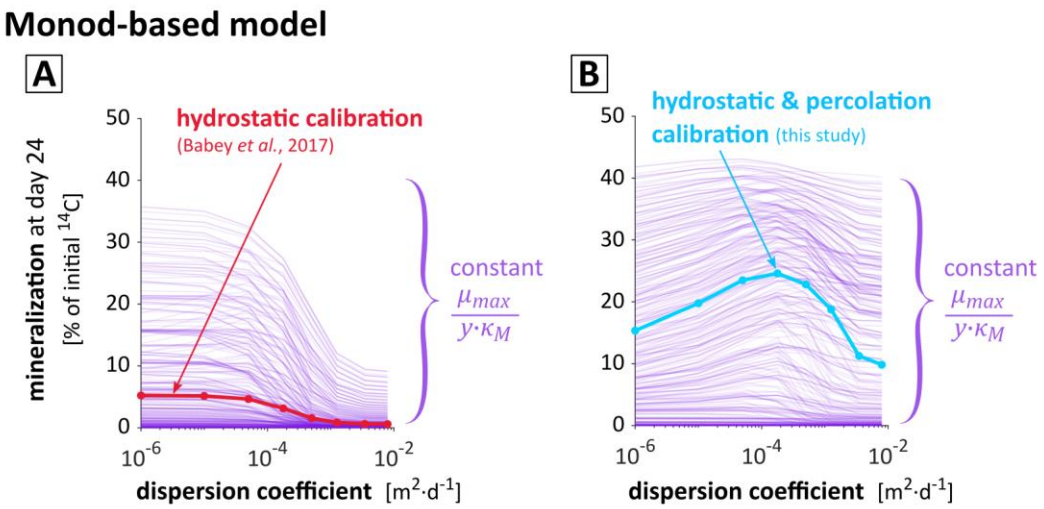

Fig. 4. Influence of the dispersion coefficient d_{disp} on mineralization predicted at day 24 $m_{CO2}(t=24)$ for the biological model calibrated on the sole hydrostatic experiments (**A**, thick red line) and on both hydrostatic and percolation experiments (**B**, thick blue line). The thin mauves lines correspond to parameter sets with the same specific maximum uptake efficiency $(1/y)\cdot\mu_{max}/\kappa_M$ but different maximum specific uptake rate $(1/y)\cdot\mu_{max}$, accommodation rate α and initial bacterial population density $B(t=0)$. The maximum uptake efficiency is the main determinant of the dispersion leading to the highest final mineralization (see section 3.2.3) while the other biological parameters determine the corresponding mineralization level. Note that for the model calibrated on both hydrostatic and percolation experiments, the value of d_{disp} leading to the highest final mineralization (d_{disp} = 1.78 10^{-4} $m^2 \cdot d^{-1}$, thick blue line) is also equal to its calibrated value leading to the best adequacy with mineralization kinetics (**Table 2**).

3.2.2 Double control of degradation by substrate accessibility and bacterial density

The non-monotonous effect of bacterial dispersion on degradation is a surprising and key feature of the model calibrated on both hydrostatic and percolation experiments. It results from a non-monotonous substrate profile issued by the respective effects of substrate accessibility and bacterial density as illustrated on **Fig. 5**.

Without any degradation, the predicted substrate concentration had a monotonously decreasing bell-shape profile after some time of diffusion (dotted pink lines on **Fig. 5**), meaning that the substrate concentration remained always maximum in its initial location. The exposure of a single bacterium to the substrate would increase with its proximity to the source of substrate. This effect is referred to as "substrate accessibility". In the hydrostatic calibrated model, the substrate uptake by bacteria located in the initial cube created an inversion of substrate gradient (**Fig. 5A**). This gradient inversion remained however limited, and the dispersion of bacteria would likely expose them to more diluted substrate by moving them away from the substrate source, hence reducing mineralization (**Fig. 4A**). Mineralization was still mainly controlled by substrate accessibility. In the model calibrated on both hydrostatic and percolation experiments, without any bacterial dispersion, bacteria depleted the substrate in the initial cube over 5 days (**Fig. 5B**). The bacteria aggregated at their initial location consumed the substrate much faster than it was replenished by backward diffusion and dispersion, leading to an intra-population competition for substrate. The dispersion of bacteria reduced competition by diluting the highest bacterial densities, thus enhancing mineralization. In this case, mineralization was mainly controlled by bacterial density. However, if bacteria were dispersed too far, substrate accessibility became the dominant control again. Therefore, an optimal bacterial spreading exists (**Fig. 5C**) for which the decrease in substrate accessibility is compensated by the dilution of high local bacterial densities. The optimal dispersion coefficient for the 300 best-fitting parameterizations to both hydrostatic and percolation experiments (smallest J_{1234} values) was on average $d_{disp} \approx 2\ 10^{-5}\ m^2 \cdot d^{-1}$ (**Fig. S7**), corresponding to a root-mean-square spreading of 1 to 2 mm by percolation event.

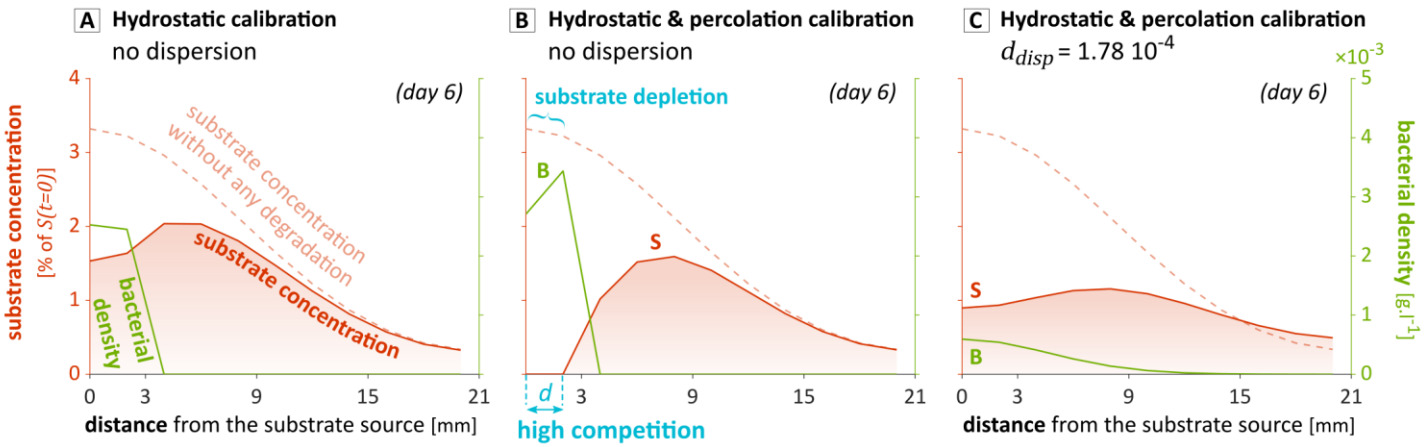

Fig. 5. Predicted substrate and bacterial concentration profiles after some time of diffusion and dispersion in the conditions of heterogeneous percolation experiment where bacteria and substrate are initially located exclusively in the central cube (between 0 and 3 mm). Results are simulated on a 9 × 18 × 18 grid obtained by subdividing the 3 × 6 × 6 grid used for the screenings. The results are represented for the parameter set calibrated on the sole hydrostatic experiment (**A**), and for the biological parameter set calibrated on both hydrostatic and percolation experiments, without dispersion (**B**) and with the calibrated dispersion (**C**). On one hand, bacteria are exposed to smaller substrate concentrations if they are far from the source (right part of the graphs). On the other hand, bacteria undergo competition if they are too close from each other (left part of the graphs). In (**B**), the bacteria aggregated below d consume the substrate faster than it is replenished by backward diffusion and dispersion.

3.2.3 Effect of bacterial uptake efficiency on the impact of dispersion on degradation

A non-monotonous substrate concentration profile only occurs when bacterial degradation locally depletes the substrate faster than it is replenished by diffusion. This area of high local competition results from high local densities of bacteria with high competiveness. Bacterial competiveness is related to their maximum uptake efficiency $(1/y)\cdot\mu_{max}/\kappa_M$, which also describes their capacity to maintain their activity and growth under diluted substrate concentrations (Healey, 1980; Button, 1991; Lobry et al., 1992). Bacteria with high maximum uptake efficiency were thus expected to benefit more from dispersion. **Fig. 6** shows the optimal

dispersion coefficient as a function of the maximum uptake efficiency, all other parameters equal to those of the model calibrated on both hydrostatic and percolation experiments. For maximum uptake efficiencies smaller than 30 $l \cdot g^{-1} \cdot d^{-1}$, dispersion did not enhance degradation, and the optimal dispersion was hence zero. For larger efficiencies, the optimal dispersion coefficient increased with the maximum uptake efficiency. When the maximum uptake efficiency increased, degradation shifted from being regulated by substrate accessibility to being regulated by bacterial densities, because bacteria were both more prone to competition between themselves and more efficient under diluted substrate conditions. In other words, the detrimental proximity to other bacteria became more constraining than the beneficial proximity to the source. This positive effect of the maximum uptake efficiency on the impact of bacterial dispersion on degradation was a general relationship common to all parameterizations (**Fig. S8**).

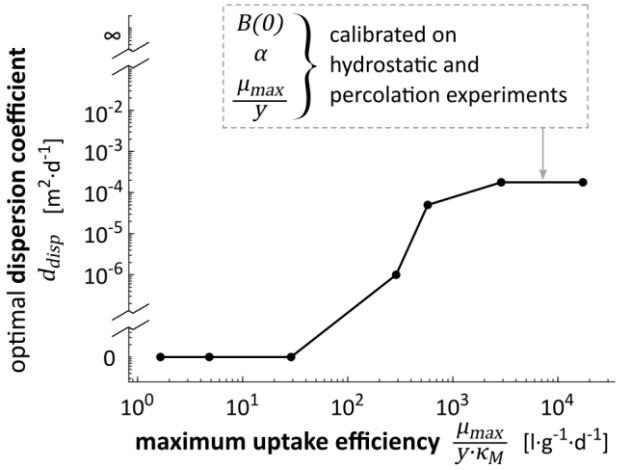

Fig. 6. Dispersion coefficient giving the highest predicted mineralization at day 24 as a function of maximum uptake efficiency, all other parameters equal to those of the model calibrated on both hydrostatic and percolation experiments.

3.3. The Contois-based model as an alternative to Monod

Given that degradation is controlled by both substrate concentrations and bacterial densities, and that their relative importance is modulated by bacterial uptake efficiency at the lowest substrate concentration,

$(1/y)\cdot\mu_{max}/\kappa_M$, we investigated the relevance of the model of Contois by applying the calibration methodology of section 2.2 as used in section 3.1. The interest of the Contois growth law (Eq. (8)) is to include the regulation by density in the expression of the uptake efficiency at the lowest substrate concentration, then equal to $(1/y)\cdot\mu_{max}/(B(t)\cdot\kappa_C)$.

The results show that the Contois-based model has three advantages. First, the 1% best-fitting parameterizations of the Contois-based model (smallest J_{1234} values) captured the degradation dynamics better than the 1% best-fitting parameterizations of the Monod-based model (**Fig. S9**). The calibrated Contois-based model had an overall discrepancy of J_{1234} = 0.022 (**Fig. 7**), smaller than the lowest value of J_{1234} = 0.032 obtained for the calibrated Monod-based model (**Fig. 3**). Second, the smallest discrepancies for the heterogeneous percolation experiment became correlated with the smallest discrepancies for the homogeneous experiments. For any biological parameter set calibrated in homogeneous conditions, there was a value of dispersion coefficient d_{disp} that made it match the heterogeneous percolation experiment. It was not the case for the Monod-based calibrated parameter sets (**Fig. S10**). It is an important advantage as it confers a better capacity to predict degradation kinetics under dispersive conditions, once calibrated in high-densities homogeneous conditions. Third, the dependence of the final mineralization on the dispersion coefficient became mostly limited, especially for the calibrated model (**Fig. 8**, thick blue line). This is because, at low substrate concentrations, the number of active bacteria in a soil volume is exactly counterbalanced by the regulation of their uptake efficiency by population density (Eq. (8)), resulting in limited effects of bacterial spreading on overall mineralization (**Fig. 8**, constant part of the curves). Note that variations can appear when the saturation effect of the ratio S/B on the specific activity or the accommodation delay α decouple the activity from the bacterial density. The lower dependence of mineralization on dispersion

shows that the effects of dispersion on the final cumulated mineralization are included in the Contois-based model more than in the Monod-based model, providing better modelling perspectives.

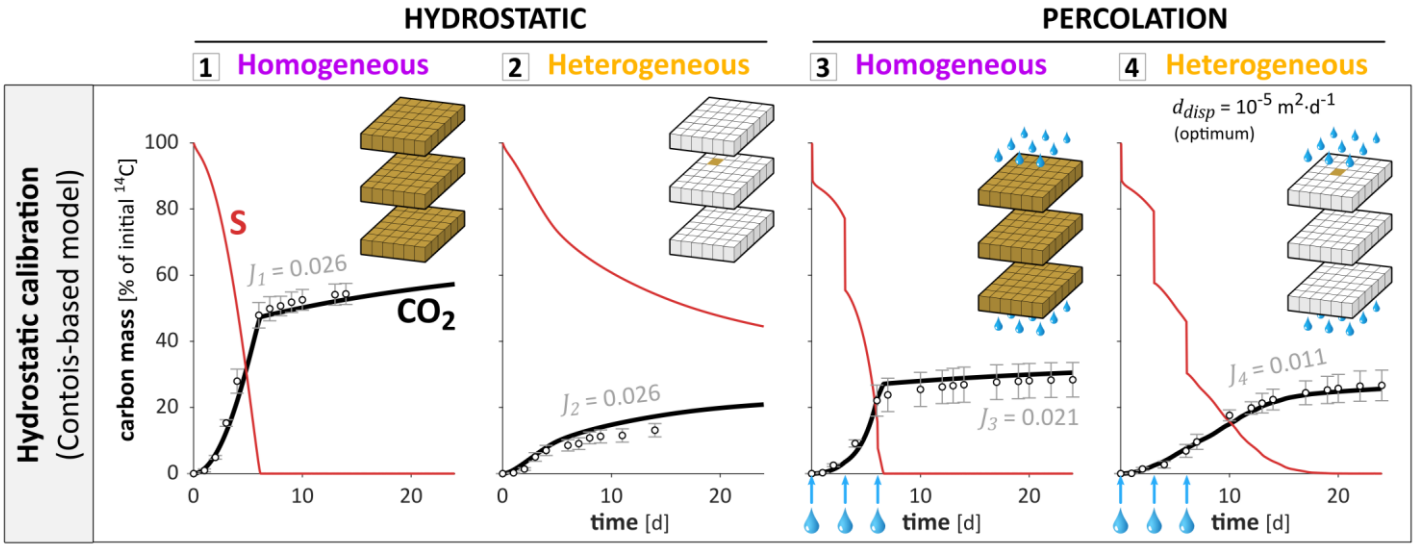

Fig. 7. Mineralization dynamics predicted with the Contois-based model calibrated on both hydrostatic and percolation experiments. For representation and legend, see **Fig. 3**. The carbon balance among the different pools is detailed in **Fig. S5**.

Despite these advantages, Contois models have also a classical drawback with the diverging efficiency of bacteria at low densities (Gleeson, 1994; Abrams, 2015). Predicted uptake efficiencies of dispersed bacteria can reach extremely high values, which do not correspond to any physical nor biochemical process. In the soil conditions represented by the experiments, it was not however critical, as these extremely high uptake efficiencies corresponded to a negligible fraction of bacteria mostly exposed to a negligible fraction of substrate.

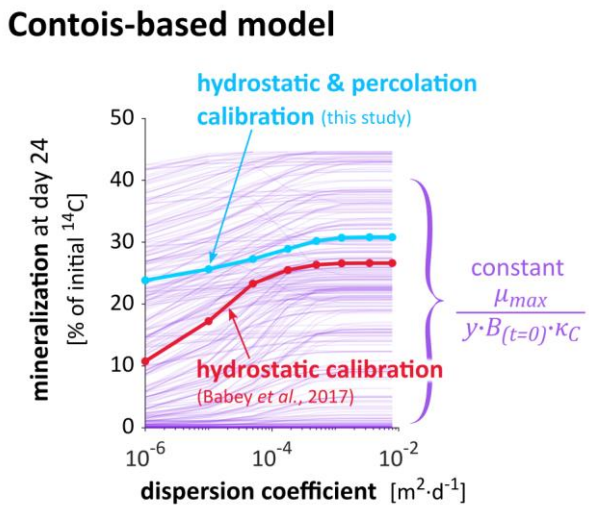

Fig. 8. Influence of the dispersion coefficient on mineralization at day 24 for the Contois-based models calibrated on the sole hydrostatic experiments (thick red line) and on both hydrostatic and percolation experiments (thick blue line). For representation and legend, see **Fig. 4**.

4. Discussion

4.1. Relevance of density control to 2,4-D degradation and soil carbon cycling

4.1.1 Density control of soil oligotroph bacteria

Bulk soil and highly-diluted environments are usually found to be dominated by bacteria with high maximum uptake efficiency, named oligotrophs (Fierer et al., 2007; Nunan et al., 2020). Their high maximum uptake efficiency differentiates their life-history strategies and conditions their ability to thrive in resource poor environments (Button, 1993), also assimilated to K-strategy (Tecon and Or, 2017), by opposition to copiotrophic bacteria adapted to rich environments (r-strategy). The maximum uptake efficiency values of the 1% best-fitting parameter sets were of the order of 10^3-10^4 $l \cdot g^{-1} \cdot d^{-1}$ (volume of water per mass of bacteria per unit of time), within the range proposed by Button (1991) to define oligotrophs. Similar or higher maximum uptake efficiency values of the order of 10^4-10^5 $l \cdot g^{-1} \cdot d^{-1}$ have been reported for soil oligotrophs

427 (Ohta and Taniguchi, 1988; Zelenev et al., 2005). Values up to 1.64 10^5 have been reported by Tuxen et al.
428 (2002) for 2,4-D degraders in an aerobic aquifer, for bacteria 1.6 times smaller in average than the ones we
429 considered (Balkwill et al., 1988). The high maximum uptake efficiencies predicted in section 3.1 for the
430 best-fitting parameterizations thus seem to be a plausible common metabolic trait not only among 2,4-D
431 degraders but also soil bacteria. It suggests that density control might be appropriate for a broad range of
432 soil bacteria, which would benefit from dispersion as suggested by **Fig. 6**, even under the low bacterial
433 densities observed in bulk soils (Raynaud and Nunan, 2014; Kuzyakov and Blagodatskaya, 2015). Conversely,
434 this striking density regulation might be one of the main limitations of the overall population densities in
435 soils. Note that this density regulation occurs within a single population with homogeneous biological
436 constants. Spatial heterogeneities and low substrate concentrations may shift competition from
437 inter-population to inter-individual as also reported by Roller and Schmidt (2015). Reciprocally, we expect
438 than, in rich environments dominated by copiotrophs (such as rhizosphere), substrate accessibility might be
439 more critical than bacterial density.

440 *4.1.2 A new perspective on Regulatory Gate hypothesis*

441 Density regulation might contribute to explain the common paradox of the apparent uncoupling between
442 the overall mineralization of a soil volume and the size of its microbial population (Kemmitt et al., 2008). The
443 rate of soil C mineralization remains the same even if 90% of the microbial decomposers are killed. The
444 Regulatory Gate hypothesis is commonly cited to explain this observation, where mineralization is assumed
445 to be controlled by an abiotic process that limits the availability of the substrate, resulting in a mineralization
446 independent of the degrader abundance. We propose that the density regulation of decomposition in
447 oligotrophic environments contribute to this phenomenon. The density regulation reduces the dependence
448 of the overall C mineralization on degrader abundance, as any increase of population density
449 counterbalances the effect of the increased population size. The involved abiotic process, namely the

substrate diffusion backward to bacteria (see section 3.2), becomes limiting specifically in situations of high bacterial competition.

4.2. Ratio-dependent modeling in soils

4.2.1 Relevance of Contois-based model in soils

To the best of our knowledge, ratio-dependent growth models such as Contois model have not yet been considered to model microbial degradation in soils. However, the Contois growth equation is generally accepted to be more appropriate than the Monod equation for modeling microbial ecosystems, immobilized cultures or heterogeneous spatial distributions (Arditi and Saiah, 1992; Harmand and Godon, 2007), which all characterize soils. It has also been widely used to model anaerobic digestion of organic wastes and has been related to kinetic restrictions by surface processes (Nelson and Holder, 2009). In fact, the regulation of individual activity by population density has long been recognized among various fields of biology (Hammond, 1938; Read, 1951; Contois, 1959) and has frequently been justified as a “crowding effect” associated with high population densities leading to competition for substrate (Lobry and Harmand, 2006; Harmand and Godon, 2007; Krichen et al., 2018). However, little is known about possible density regulation when apparent microbial densities are low, as is observed in bulk soil (Raynaud and Nunan, 2014; Kuzyakov and Blagodatskaya, 2015), although some studies have mentioned ratio-dependence in highly-diluted environments such as aquifers (Hansen et al., 2017). As discussed in section 4.1.1, the high oligotrophic capacities commonly observed for soil bacteria are relevant to consider the importance of density control in soils. In comparison with the substrate-dependent growth law of Monod, Contois ratio-dependence includes not only the effect of competition for substrate at the scale of measurement, it can also reasonably reflect the spatial variability of bacterial distributions at finer scales related to their high degree of local aggregation in microcolonies (Raynaud and Nunan, 2014). It has been shown independently that the fast local aggregation of bacteria leads naturally to ratio-dependent models (Haegeman and Rapaport, 2008;

Rapaport, 2018). Moreover, ratio-dependence may include as well the cumulative effects of ecological interactions other than competition (Sibly and Hone, 2002). As also argued in section 3.3, ratio-dependence may facilitate degradation modeling at least in the soil conditions typical of the experiments analyzed here, since it reduces the need to determine which scale is relevant for measuring the spatial distributions and densities of bacteria in soil, a major limit of current knowledge (Juyal et al., 2019).

4.2.2 High transient bacterial maximum uptake efficiencies

A key feature of the Contois-based model is that the maximum uptake efficiency can locally reach higher values than with the Monod model (Eq. (8) and section 3.3). To some extent, high values are expected to be physically and biologically plausible when biological systems approach the theoretical collision frequency rate between bacteria and solutes and reach the "collisional limit" (Koch, 1971; Abbott and Nelsestuen, 1988). This theoretical collision frequency rate, expressed by $4\pi r_B D_S$ with r_B the radius of 2,4-D degraders and D_S the molecular diffusion coefficient (see section S.5) (Smoluchowski, 1918; Koch, 1971), was equal to 2.32 10^6 $l \cdot g^{-1} \cdot d^{-1}$ in our system, assuming that bacteria have a mean diameter of 0.75 µm and an average cell mass of 2.8 10^{-13} g (Dechesne et al., 2010). Such high values agree with theoretical values estimated for marine bacteria and experimental values of 2.4 10^6 $l \cdot g^{-1} \cdot d^{-1}$ proposed by Button (1993). Were such values reached by some soil bacteria, it would expose the need to consider population density when measuring maximum uptake efficiency to avoid underestimating it by unintentionally including density regulation into the apparent measure of maximum uptake efficiency.

4.3. Hypothetical relationship between bacterial metabolic traits and their spatial strategies

Density regulation might be at the origin of a relationship between bacterial oligotrophy, their location in soil and their mobility strategy. Soil copiotroph bacteria have a maximum uptake efficiency mostly between

100 $l \cdot g^{-1} \cdot d^{-1}$ (Button, 1991) and 800 $l \cdot g^{-1} \cdot d^{-1}$ (Daugherty and Karel, 1994; Zelenev et al., 2005). For copiotrophs with maximum uptake efficiency values below 288 $l \cdot g^{-1} \cdot d^{-1}$, bacterial dispersion was largely detrimental (**Fig. 4A**, **Fig. 6**), in agreement with the results of Pagel et al. (2020) suggesting that copiotrophs have more aggregated distributions than oligotrophs. The negligible mineralization even without dispersion (**Fig. 3-A4**, **Fig. S8**) also highlights that copiotrophs are particularly inefficient for degrading substrates that diffuses in the environment, as also evidenced by Babey et al. (2017). To remain significantly active, soil copiotrophs are likely to remain immobile in the close surroundings of the substrate source or any immobile substrate, likely attached to surfaces or embedded in EPS matrices. If not, they would be dispersed towards more diluted area where their low maximum uptake efficiency would result in negligible uptake. On the contrary, to survive and develop, soil oligotrophs should be able to easily disperse and escape high competition areas. Given that soil is a poor and heterogeneous environment, this dispersion would be essentially passive (Nunan et al., 2020), like through advective processes. We therefore suggest the existence of a theoretical relation between proximity to substrate sources (respectively remoteness), copiotrophy (respectively oligotrophy) and attachment (respectively mobility).

5. Conclusions

Heterogeneous distributions of degraders and substrate in soils strongly control soil organic matter degradation through their interactions with the bacterial metabolic activity. Taking 2,4-D as a model organic solute substrate for soil bacteria, we investigated the coupled effects of bacteria and substrate distributions on one side and bacterial metabolic traits on the other side on substrate degradation. The analysis of experiments previously performed with contrasted spreading conditions of both bacteria and substrate reveals that, in addition to the proximity of bacteria to high substrate concentrations (substrate accessibility), mineralization is also surprisingly controlled by the remoteness between bacteria (bacteria density) even under the low bacterial densities commonly observed in bulk soils. Moreover, the impact of bacterial

dispersion on solute substrate degradation can shift from negative to positive depending on the bacterial maximum uptake efficiency. Soil oligotrophs activity would be mostly determined by bacterial density rather than by substrate accessibility, echoing the population size paradox regularly observed. It follows that the ratio-dependent Contois model might be more relevant to model soil mineralization in the heterogeneous conditions investigated than the substrate-dependent Monod model. To predict the impact of spatial distributions on degradation in oligotrophic soil, and more particularly the impact of bacterial dispersion, we suggest that bacterial densities might be a more useful measurement than the volumes of soil devoid or occupied with bacteria. With respect to the current lack of direct microscale data on microbial processes and distributions, we propose some key perspectives on the bacterial kinetics and distributions.

Declaration of competing interest

The authors declare that they have no known competing financial interests or personal relationships that could have appeared to influence the work reported in this paper.

Acknowledgements

This work was supported by the Agence Nationale de la Recherche through the project “Soilμ-3D” [grant number ANR-15-CE01-0006].

Appendix A. Supplementary data

534 # References

535 Abbott, A.J., Nelsestuen, G.L., 1988. The collisional limit: an important consideration for membrane-
536 associated enzymes and receptors. The FASEB Journal 2, 2858–2866.
537 https://doi.org/10.1096/fasebj.2.13.2844615

538 Abrams, P.A., 2015. Why ratio dependence is (still) a bad model of predation: Ratio-dependent predation.
539 Biological Reviews 90, 794–814. https://doi.org/10.1111/brv.12134

540 Arditi, R., Saiah, H., 1992. Empirical evidence of the role of heterogeneity in ratio-dependent consumption.
541 Ecology 73, 1544–1551. https://doi.org/10.2307/1940007

542 Babey, T., Vieublé Gonod, L., Rapaport, A., Pinheiro, M., Garnier, P., de Dreuzy, J.-R., 2017. Spatiotemporal
543 simulations of 2,4-D pesticide degradation by microorganisms in 3D soil-core experiments.
544 Ecological Modelling 344, 48–61. https://doi.org/10.1016/j.ecolmodel.2016.11.006

545 Bælum, J., Henriksen, T., Hansen, H.C.B., Jacobsen, C.S., 2006. Degradation of 4-chloro-2-
546 methylphenoxyacetic acid in top- and subsoil is quantitatively linked to the class III tfdA gene.
547 Applied and Environmental Microbiology 72, 1476–1486. https://doi.org/10.1128/AEM.72.2.1476-
548 1486.2006

549 Bælum, J., Nicolaisen, M.H., Holben, W.E., Strobel, B.W., Sørensen, J., Jacobsen, C.S., 2008. Direct analysis
550 of tfdA gene expression by indigenous bacteria in phenoxy acid amended agricultural soil. The ISME
551 Journal 2, 677–687. https://doi.org/10.1038/ismej.2008.21

552 Balkwill, D.L., Leach, F.R., Wilson, J.T., McNabb, J.F., White, D.C., 1988. Equivalence of microbial biomass
553 measures based on membrane lipid and cell wall components, adenosine triphosphate, and direct
554 counts in subsurface aquifer sediments. Microbial Ecology 16, 73–84.
555 https://doi.org/10.1007/BF02097406

556 Boivin, A., Amellal, S., Schiavon, M., van Genuchten, M.Th., 2005. 2,4-dichlorophenoxyacetic acid (2,4-D)
557 sorption and degradation dynamics in three agricultural soils. Environmental Pollution 138, 92–99.
558 https://doi.org/10.1016/j.envpol.2005.02.016

559 Breitenbeck, G.A., Yang, H., Dunigan, E.P., 1988. Water-facilitated dispersal of inoculant Bradyrhizobium
560 japonicum in soils. Biology and Fertility of Soils 7, 58–62. https://doi.org/10.1007/BF00260733

561 Bünemann, E.K., Bongiorno, G., Bai, Z., Creamer, R.E., De Deyn, G., de Goede, R., Fleskens, L., Geissen, V.,
562 Kuyper, T.W., Mäder, P., Pulleman, M., Sukkel, W., van Groenigen, J.W., Brussaard, L., 2018. Soil
563 quality – A critical review. Soil Biology and Biochemistry 120, 105–125.
564 https://doi.org/10.1016/j.soilbio.2018.01.030

565 Button, D.K., 1978. On the theory of control of microbial growth kinetics by limiting nutrient
566 concentrations. Deep Sea Research 25, 1163–1177. https://doi.org/10.1016/0146-6291(78)90011-5

567 Button, D.K., 1983. Differences between the kinetics of nutrient uptake by micro-organisms, growth and
568 enzyme kinetics. Trends in Biochemical Sciences 8, 121–124. https://doi.org/10.1016/0968-
569 0004(83)90232-3

570 Button, D.K., 1991. Biochemical basis for whole-cell uptake kinetics: specific affinity, oligotrophic capacity,
571 and the meaning of the michaelis constant. Applied and Environmental Microbiology 57, 2033–
572 2038.

573 Button, D.K., 1993. Nutrient-limited microbial growth kinetics: overview and recent advances. Antonie van
574 Leeuwenhoek 63, 225–235. https://doi.org/10.1007/BF00871220

575 Cheyns, K., Mertens, J., Diels, J., Smolders, E., Springael, D., 2010. Monod kinetics rather than a first-order
576 degradation model explains atrazine fate in soil mini-columns: Implications for pesticide fate
577 modelling. Environmental Pollution 158, 1405–1411. https://doi.org/10.1016/j.envpol.2009.12.041

578 Contois, D.E., 1959. Kinetics of bacterial growth: relationship between population density and specific
579 growth rate of continuous cultures. Journal of General Microbiology 21, 40–50.
580 https://doi.org/10.1099/00221287-21-1-40

581 Daugherty, D.D., Karel, S.F., 1994. Degradation of 2,4-dichlorophenoxyacetic acid by Pseudomonas cepacia
582 DBOl(pRO101) in a dual-substrate chemostat. Applied and Environmental Microbiology 60, 3261–
583 3267.

584 Dechesne, A., Owsianiak, M., Bazire, A., Grundmann, G.L., Binning, P.J., Smets, B.F., 2010. Biodegradation in
585 a partially saturated sand matrix: compounding effects of water content, bacterial spatial
586 distribution, and motility. Environmental Science & Technology 44, 2386–2392.
587 https://doi.org/10.1021/es902760y

588 Dechesne, A., Badawi, N., Aamand, J., Smets, B.F., 2014. Fine scale spatial variability of microbial pesticide
589 degradation in soil: scales, controlling factors, and implications. Frontiers in Microbiology 5, 667.
590 https://doi.org/10.3389/fmicb.2014.00667

591 Don, R.H., Weightman, A.J., 1985. Transposon mutagenesis and cloning analysis of the pathways for
592 degradation of 2,4-dichlorophenoxyacetic acid and 3-chlorobenzoate in Alcaligenes eutrophus
593 JMP134(pJP4). Journal of Bacteriology 161, 85–90.

594 Dungait, J.A.J., Hopkins, D.W., Gregory, A.S., Whitmore, A.P., 2012. Soil organic matter turnover is
595 governed by accessibility not recalcitrance. Global Change Biology 18, 1781–1796.
596 https://doi.org/10.1111/j.1365-2486.2012.02665.x

597 Fierer, N., Bradford, M.A., Jackson, R.B., 2007. Toward an ecological classification of soil bacteria. Ecology
598 88, 1354–1364. https://doi.org/10.1890/05-1839

599 Gleeson, S.K., 1994. Density dependence is better than ratio dependence. Ecology 75, 1834–1835.
600 https://doi.org/10.2307/1939642

Haegeman, B., Rapaport, A., 2008. How flocculation can explain coexistence in the chemostat. Journal of Biological Dynamics 2, 1–13. https://doi.org/10.1080/17513750801942537

Hammond, E.C., 1938. Biological effects of population density in lower organisms. The Quarterly Review of Biology 13, 421–438. http://www.jstor.org/stable/2808555

Hansen, S.K., Pandey, S., Karra, S., Vesselinov, V.V., 2017. CHROTRAN: A mathematical and computational model for in situ heavy metal remediation in heterogeneous aquifers. ArXiv:1703.01381 [q-Bio].

Harmand, J., Godon, J.J., 2007. Density-dependent kinetics models for a simple description of complex phenomena in macroscopic mass-balance modeling of bioreactors. Ecological Modelling 200, 393–402. https://doi.org/10.1016/j.ecolmodel.2006.08.012

Healey, F.P., 1980. Slope of the Monod equation as an indicator of advantage in nutrient competition. Microbial Ecology 5, 281–286. http://www.jstor.org/stable/4250586

Holden, P.A., Firestone, M.K., 1997. Soil microorganisms in soil cleanup: How can we improve our understanding? Journal of Environment Quality 26, 32–40. https://doi.org/10.2134/jeq1997.00472425002600010006x

Iserles, A., 2009. A first course in the numerical analysis of differential equations, Cambridge University Press. ed.

Juyal, A., Otten, W., Falconer, R., Hapca, S., Schmidt, H., Baveye, P.C., Eickhorst, T., 2019. Combination of techniques to quantify the distribution of bacteria in their soil microhabitats at different spatial scales. Geoderma 334, 165–174. https://doi.org/10.1016/j.geoderma.2018.07.031

Kemmitt, S.J., Lanyon, C.V., Waite, I.S., Wen, Q., Addiscott, T.M., Bird, N.R.A., O'Donnell, A.G., Brookes, P.C., 2008. Mineralization of native soil organic matter is not regulated by the size, activity or composition of the soil microbial biomass—a new perspective. Soil Biology and Biochemistry 40, 61–73. https://doi.org/10.1016/j.soilbio.2007.06.021

Koch, A.L., 1971. The adaptive responses of Escherichia coli to a feast and famine existence, in: Advances in Microbial Physiology. Elsevier, pp. 147–217. https://doi.org/10.1016/S0065-2911(08)60069-7

König, S., Vogel, H.-J., Harms, H., Worrich, A., 2020. Physical, chemical and biological effects on soil bacterial dynamics in microscale models. Frontiers in Ecology and Evolution 8, 53. https://doi.org/10.3389/fevo.2020.00053

Krichen, E., Harmand, J., Torrijos, M., Godon, J.J., Bernet, N., Rapaport, A., 2018. High biomass density promotes density-dependent microbial growth rate. Biochemical Engineering Journal 130, 66–75. https://doi.org/10.1016/j.bej.2017.11.017

Kuzyakov, Y., Blagodatskaya, E., 2015. Microbial hotspots and hot moments in soil: Concept & review. Soil Biology and Biochemistry 83, 184–199. https://doi.org/10.1016/j.soilbio.2015.01.025

Lobry, C., Harmand, J., 2006. A new hypothesis to explain the coexistence of n species in the presence of a single resource. Comptes Rendus Biologies 329, 40–46. https://doi.org/10.1016/j.crvi.2005.10.004

Lobry, J.R., Flandrois, J.P., Carret, G., Pave, A., 1992. Monod's bacterial growth model revisited. Bulletin of Mathematical Biology 54, 117–122. https://doi.org/10.1007/BF02458623

Madsen, E.L., Alexander, M., 1982. Transport of Rhizobium and Pseudomonas through Soil. Soil Science Society of America Journal 46, 557–560. https://doi.org/10.2136/sssaj1982.03615995004600030023x

Monod, J., 1949. The growth of bacterial cultures. Annual Review of Microbiology 3, 371–394. https://doi.org/10.1146/annurev.mi.03.100149.002103

Nelson, M.I., Holder, A., 2009. A fundamental analysis of continuous flow bioreactor models governed by Contois kinetics. II. Reactor cascades. Chemical Engineering Journal 149, 406–416. https://doi.org/10.1016/j.cej.2009.01.028

Nunan, N., Young, I.M., Crawford, J.W., Ritz, K., 2007. Bacterial interactions at the microscale - Linking habitat to function in soil, in: Franklin, R., Mills, A. (Eds.), The Spatial Distribution of Microbes in the Environment. Springer, Dordrecht, pp. 61–85.

Nunan, N., Schmidt, H., Raynaud, X., 2020. The ecology of heterogeneity: soil bacterial communities and C dynamics. Philosophical Transactions of the Royal Society B: Biological Sciences 375, 20190249. https://doi.org/10.1098/rstb.2019.0249

Ohta, H., Taniguchi, S., 1988. Growth characteristics of the soil oligotrophic bacterium: Agromonas oligotrophica JCM 1494 on diluted nutrient broth. The Journal of General and Applied Microbiology 34, 349–353. https://doi.org/10.2323/jgam.34.349

Pagel, H., Kriesche, B., Uksa, M., Poll, C., Kandeler, E., Schmidt, V., Streck, T., 2020. Spatial control of carbon dynamics in soil by microbial decomposer communities. Frontiers in Environmental Science 8, 2. https://doi.org/10.3389/fenvs.2020.00002

Pallud, C., Dechesne, A., Gaudet, J.P., Debouzie, D., Grundmann, G.L., 2004. Modification of spatial distribution of 2,4-dichlorophenoxyacetic acid degrader microhabitats during growth in soil columns. Applied and Environmental Microbiology 70, 2709–2716. https://doi.org/10.1128/AEM.70.5.2709-2716.2004

Patarinska, T., Dochain, D., Agathos, S.N., Ganovski, L., 2000. Modelling of continuous microbial cultivation taking into account the memory effects. Bioprocess Engineering 22, 517–527. https://doi.org/10.1007/s004499900095

Pieper, D.H., Reineke, W., Engesser, K.-H., Knackmuss, H.-J., 1988. Metabolism of 2,4-dichlorophenoxyacetic acid, 4-chloro-2-methylphenoxyacetic acid and 2-methylphenoxyacetic acid by Alcaligenes eutrophus JMP 134. Archives of Microbiology 150, 95–102. https://doi.org/10.1007/BF00409724

Pinheiro, M., Garnier, P., Beguet, J., Martin Laurent, F., Vieublé Gonod, L., 2015. The millimetre-scale distribution of 2,4-D and its degraders drives the fate of 2,4-D at the soil core scale. Soil Biology and Biochemistry 88, 90–100. https://doi.org/10.1016/j.soilbio.2015.05.008

Pinheiro, M., Pagel, H., Poll, C., Ditterich, F., Garnier, P., Streck, T., Kandeler, E., Vieublé Gonod, L., 2018. Water flow drives small scale biogeography of pesticides and bacterial pesticide degraders - A microcosm study using 2,4-D as a model compound. Soil Biology and Biochemistry 127, 137–147. https://doi.org/10.1016/j.soilbio.2018.09.024

Poll, C., Ingwersen, J., Stemmer, M., Gerzabek, M.H., Kandeler, E., 2006. Mechanisms of solute transport affect small-scale abundance and function of soil microorganisms in the detritusphere. European Journal of Soil Science 57, 583–595. https://doi.org/10.1111/j.1365-2389.2006.00835.x

Rapaport, A., 2018. Properties of the chemostat model with aggregated biomass. European Journal of Applied Mathematics 29, 972–990. https://doi.org/10.1017/S0956792518000141

Raynaud, X., Nunan, N., 2014. Spatial Ecology of Bacteria at the Microscale in Soil. PLoS ONE 9, e87217. https://doi.org/10.1371/journal.pone.0087217

Read, C.P., 1951. The “Crowding Effect” in Tapeworm Infections. The Journal of Parasitology 37, 174–178. https://doi.org/10.2307/3273449

Roller, B.R., Schmidt, T.M., 2015. The physiology and ecological implications of efficient growth. The ISME Journal 9, 1481–1487. https://doi.org/10.1038/ismej.2014.235

Shampine, L.F., Reichelt, M.W., 1997. The MATLAB ODE Suite. SIAM Journal on Scientific Computing 18, 1–22. https://doi.org/10.1137/S1064827594276424

Sibly, R.M., Hone, J., 2002. Population growth rate and its determinants: an overview. Philosophical Transactions of the Royal Society of London. Series B: Biological Sciences 357, 1153–1170. https://doi.org/10.1098/rstb.2002.1117

692 Sinton, G.L., Fan, L.T., Erickson, L.E., Lee, S.M., 1986. Biodegradation of 2,4-D and related xenobiotic
693 compounds. Enzyme and Microbial Technology 8, 395–403. https://doi.org/10.1016/0141-
694 0229(86)90145-6

695 Smoluchowski, M. v, 1918. Versuch einer mathematischen Theorie der Koagulationskinetik kolloider
696 Lösungen. Zeitschrift für Physikalische Chemie 92U, 129–168. https://doi.org/10.1515/zpch-1918-
697 9209

698 Tecon, R., Or, D., 2017. Biophysical processes supporting the diversity of microbial life in soil. FEMS
699 Microbiology Reviews 41, 599–623. https://doi.org/10.1093/femsre/fux039

700 Tuxen, N., de Lipthay, J.R., Albrechtsen, H.-J., Aamand, J., Bjerg, P.L., 2002. Effect of exposure history on
701 microbial herbicide degradation in an aerobic aquifer affected by a point source. Environmental
702 Science & Technology 36, 2205–2212. https://doi.org/10.1021/es0113549

703 Vieublé Gonod, L., Chenu, C., Soulas, G., 2003. Spatial variability of 2,4-dichlorophenoxyacetic acid (2,4-D)
704 mineralisation potential at a millimetre scale in soil. Soil Biology and Biochemistry 35, 373–382.
705 https://doi.org/10.1016/S0038-0717(02)00287-0

706 Young, I.M., Crawford, J.W., Nunan, N., Otten, W., Spiers, A., 2008. Chapter 4 Microbial distribution in soils,
707 in: Advances in Agronomy. Elsevier, pp. 81–121. https://doi.org/10.1016/S0065-2113(08)00604-4

708 Zelenev, V.V., van Bruggen, A.H.C., Semenov, A.M., 2005. Modeling wave-like dynamics of oligotrophic and
709 copiotrophic bacteria along wheat roots in response to nutrient input from a growing root tip.
710 Ecological Modelling 188, 404–417. https://doi.org/10.1016/j.ecolmodel.2005.01.046

711 **Appendix A. Supplementary Data**